16th Australasian Fluid Mechanics Conference
Crown Plaza, Gold Coast, Australia
2-7 December 2007

The effect of short-crested wave phase on a concentric porous cylinder system in the wind blowing open sea

H. Song and L. Tao

Griffith School of Engineering
Griffith University, Gold Coast, Queensland, 4222, Australia

Abstract

Cylindrical structures are widely employed in the offshore engineering. How to protect the structures in real sea environment is a vital issue for scientists and engineers. In this paper, the interaction of short-crested waves with a concentric surface-piercing two-cylinder system is studied based on linear wave theory using the scaled boundary finite-element method (SBFEM), a novel semi-analytical method with the advantages of combining the finite-element method (FEM) with the boundary-element method (BEM). The interior cylinder is impermeable and the exterior cylinder is thin and porous to protect the interior cylinder. Both of cylinders are bottom mounted. Wave elevation in the annular region is found dependent on the short-crested phase, and the total forces fluctuate as the phase changes. It is further revealed that the maximum total forces are smaller than those induced by plane waves and standing waves with the same total wave number.

Introduction

In order to reduce the direct wave impact, coastal and offshore structures are often constructed with one or more protective porous layers. Examples are rock-filled porous breakwaters outside harbours, concentric porous outer protective structure with the main structure in its interior. One such application is the successful Ekofisk gravity offshore structure in the North Sea. For these reasons, wave motion through a porous structure has attracted considerable interests among researchers in coastal and ocean engineering.

In addition to the porous wavemaker theory of Chwang [1] and subsequent works, investigations on waves past a porous structure are primarily been concentrated on the hydrodynamic effects of a porous structure on the incoming wave trains, or wave impact on porous structures as a breakwater in a harbour (e.g., [13, 14]). In most cases, Darcy's law for a homogeneous porous medium has been applied. Yu and Chwang [13] investigated the resonance in a harbour with porous breakwaters with the wave entering at an arbitrary angle. Yu and Chwang [14] performed extensive study on the transmission characteristics of waves past a porous structure. The wave behaviour within the porous medium was also investigated. It was found that there is an optimum thickness for a porous structure beyond which any further increase of the thickness may not lead to an appreciable improvement in reducing its transmission and reflection characteristics. Wang and Ren [9] also studied the performance of a flexible and porous breakwater. Additional related work can be found in the review article of Chwang and Chan [2].

Though considerable research efforts have been devoted to the wave interaction with porous structures, relatively limited attention has been focused on the wave diffraction by a concentric bottom-mounted porous cylindrical structure, where the interior cylinder is impermeable and the exterior cylinder is thin and porous. Wang and Ren [10] investigated analytically the plane wave diffraction by the above-mentioned system. They found that hydrodynamic forces on the interior cylinder as well as wave amplitudes around the windward side of the interior cylinder are reduced compared to the case of a direct wave impact on the interior cylinder. As the annular spacing increases, the hydrodynamic force on the interior cylinder decreases. It was further shown that, as the porosity of the exterior cylinder increases, the hydrodynamic force on the interior cylinder increases. Darwiche et al. [3] also studied the wave diffraction by a two-cylinder system, with the exterior cylinder being porous only in the vicinity of free surface. Williams and Li [11] further extended the work by mounting the interior cylinder on a storage tank.

The aforementioned studies on ocean surface waves interaction with a vertical porous cylindrical structure are generally two-dimensional. In reality, however, the ocean waves are more complex, and better described by three-dimensional short-crested waves. They also commonly arise, for example, from the oblique interaction of two travelling plane waves or intersecting swell waves, from the reflection of waves at non-normal incident off a vertical seawall, as well as from diffraction about the surface boundaries of a structure of finite length. Such waves are of paramount importance in coastal and offshore engineering design. Unlike the plane waves propagating in a single direction, and the standing waves fluctuating vertically in a confined region, short-crested waves can be doubly periodic in two horizontal directions, one in the direction of propagation and the other normal to it [8].

Theoretical analysis on short-crested waves interaction with a vertical cylinder can be found in [15, 16]. Zhu [15] presented an analytic solution to the diffraction problem for a circular cylinder in short-crested waves using linear potential wave theory and revealed that the pressure distribution and wave run-up on the cylinder were quite different from those of plane incident waves. Their patterns become very complex as ka (i.e., total incident wave number k times cylinder radius a) becomes large. The hydrodynamic forces on the cylinder become smaller as the short-crestedness of the incident wave increases. Subsequently, Zhu and Moule [16] observed that the hydrodynamic force induced by short-crested waves varies with the phase angle perpendicular to the direction of wave propagation.

Recently, a semi-analytical method, called scaled boundary finite-element method (SBFEM) for solving linear partial differential equations has found successful application to soil-structure interaction problems. The SBFEM method was proposed by Song and Wolf [5] and systematically described by Wolf [12]. Combining the distinct advantages of the finite-element and boundary-element methods, only the structure boundary is discretised with surface finite-elements. This, in turn, transforms the governing partial differential equations to a set of ordinary differential equations, and solves them analytically. The method represents singularities and unbounded domains accurately and efficiently when compared to the complete finite-element method and requires no fundamental solution as needed by the boundary-element method. Fewer elements are required to obtain very accurate results [12].

Li et al. [4] solved the problem of plane wave diffraction by a vertical cylinder using SBFEM. Similar to the approach of Wolf [12] in obtaining a solution for soil-structure interaction, Li et al. [4] adopted an algebraic series to obtain the final solution. However, for low frequency waves with $ka \ll 1$ the series converges very slowly, hardly approaching to the exact solution.

Tao et al. [6] applied the SBFEM to solve short-crested waves interaction with a circular cylinder. Instead of using a power series, Tao et al. [6] chose Hankel function to solve the Helmholtz equation in the unbounded domain. The radial differential equation is solved fully analytically in all frequency ranges. Without relying on any other numerical schemes, the semi-analytical model for the plane-wave diffraction by a single circular cylinder is shown to reproduce the analytical solution for all the physical properties including wave run-up, effective inertia and drag coefficients, and total force very accurately and at very low computational cost.

Although much effort has been made on wave interaction with porous cylinders and breakwaters, works on the short-crested waves interaction with a concentric porous cylindrical structure, especially the effects of short-crested phase have been relatively few. This paper aims at this particular aspect in a quantitative manner. It will apply the SBFEM model developed in [6] to study the short-crested wave interaction with a concentric porous cylindrical structure.

Mathematical Formulation

Consider a monochromatic short-crested wave train propagating in the direction of the positive x axis. A structure consisting of two concentric fixed vertical cylinders extend from the sea bottom to above the free surface of the ocean along z axis. The origin is placed at the centre of the cylinders on the mean water surface (see Fig. 1). The exterior cylinder is made porous and the interior cylinder is impermeable. The whole fluid region is divided into two regions, the annular region Ω_1 and the region of the outside of the exterior cylinder Ω_2. The following notation have been used in the paper: Φ_j = total velocity potential, Φ^I = velocity potential of incident wave, Φ^S = velocity potential of scattered wave, k = total wave number, k_x = wave number in x direction, k_y = wave number in y direction, ω = wave frequency, h = water depth, A = amplitude of incident wave, a = interior cylinder radius, b = exterior cylinder radius, t = time, ρ = mass density of water, and g = gravitational acceleration. The subscripts $j(j=1,2)$ denote the physical parameters in the region $\Omega_j(j=1,2)$.

Assuming the fluid to be inviscid, incompressible and the flow to be irrotational, the fluid motion can be described by a velocity potential Φ_j satisfying the Laplace equation

$$\nabla^2\Phi_j = 0 \qquad \text{in} \quad \Omega_j, \tag{1}$$

subject to the combined free surface boundary condition

$$\Phi_{j,tt} + g\Phi_{j,z} = 0 \qquad \text{at} \quad z = 0, \tag{2}$$

and the bottom condition

$$\Phi_{j,z} = 0 \qquad \text{at} \quad z = -h, \tag{3}$$

where the comma in the subscript designates partial derivative with respect to the variable following the comma.

The velocity potentials can be decomposed by separating the vertical variable z and the time t from each component as

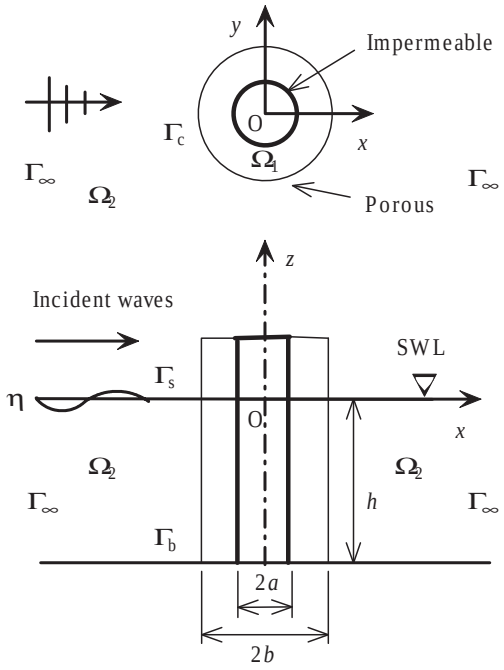

Figure 1: Wave interaction with a concentric porous cylindrical structure

$$\Phi_j(x,y,z,t) = \phi_j(x,y)Z(z)e^{-i\omega t} \qquad \text{in} \quad \Omega_j, \tag{4}$$
$$\Phi_2^I(x,y,z,t) = \phi_2^I(x,y)Z(z)e^{-i\omega t} \qquad \text{in} \quad \Omega_2, \tag{5}$$
$$\Phi_2^S(x,y,z,t) = \phi_2^S(x,y)Z(z)e^{-i\omega t} \qquad \text{in} \quad \Omega_2, \tag{6}$$

where

$$Z(z) = \frac{\cosh k(z+h)}{\cosh kh}. \tag{7}$$

This procedure leads to the sea bottom condition being automatically satisfied, and the linearised free surface boundary condition is satisfied using the following dispersion relationship

$$\omega^2 = gk\tanh kh. \tag{8}$$

The relationship between the total velocity potential, and the scattered, and incident wave velocity potentials is

$$\Phi_2 = \Phi_2^I + \Phi_2^S, \quad \phi_2 = \phi_2^I + \phi_2^S \qquad \text{in} \quad \Omega_2. \tag{9}$$

According to Taylor [7], the fluid flow passing through the porous boundary can be essentially assumed to obey Darcy's law if the boundary is made of fine pores. Thus, the porous flow velocity is linearly proportional to the pressure difference between the two sides of the porous boundary, and the boundary condition on exterior porous cylinder can be expressed as [1]

$$\phi_{1,n} = -\phi_{2,n} = iG_0k(\phi_1 - \phi_2) \quad \text{on} \quad r = b, \tag{10}$$

where $G_0 = \frac{\rho\omega d}{\mu}$, is a measure of the porous effect, μ is the coefficient of dynamic viscosity, d is a material constant having the dimension of a length, and n denotes the normal to the boundary.

The boundary-value problem is simplified as two-dimensional at the free surface. The function $\phi_2^S(x,y)$ in Ω_2 is governed by the Helmholtz equation with the boundary condition at the interface of fluid and porous cylinder, and the radiation condition at infinity, namely, the Sommerfeld condition as follows:

$$\nabla^2\phi_2^S + k^2\phi_2^S = 0 \qquad \text{in} \quad \Omega_2, \tag{11}$$

$$\phi_{2,n}^S = -iG_0k(\phi_1 - \phi_2^S - \phi_2^I) - \phi_{2,n}^I \quad \text{on} \quad r = b, \tag{12}$$

$$\lim_{kr\to\infty}(kr)^{1/2}\left(\phi_{2,r}^S - ik\phi_2^S\right) = 0 \qquad \text{in} \quad \Omega_2, \tag{13}$$

where r is the radial axis, and $i = \sqrt{-1}$.

The function $\phi_1(x,y)$ in Ω_1 is governed by the Helmholtz equation with the boundary conditions at the interface of fluid and interior solid cylinder at $r = a$ and exterior porous cylinder at $r = b$:

$$\nabla^2\phi_1 + k^2\phi_1 = 0 \qquad \text{in} \quad \Omega_1, \tag{14}$$

$$\phi_{1,n} = 0 \quad \text{on} \quad r = a, \tag{15}$$

$$\phi_{1,n} = iG_0k(\phi_1 - \phi_2^S - \phi_2^I) \quad \text{on} \quad r = b. \tag{16}$$

The velocity potential of the linear short-crested incident wave travelling principally in the positive x direction is given by the real part of [16]

$$\Phi_2^I = -\frac{igA}{\omega}Z(z)e^{i(k_xx-\omega t)}\cos(k_yy+\theta) \qquad \text{in} \quad \Omega_2, \tag{17}$$

where θ is the phase of the sinusoidal wave crests in the direction perpendicular to the direction of wave propagation.

Eqs (11)-(16) constitute two sets of the governing equation and boundary conditions for the diffraction of short-crested waves by concentric vertical porous cylindrical structure, corresponding to boundary value problems in a bounded domain and an unbounded domain respectively. After obtaining ϕ_2^S, Φ_2 and Φ_1 by solving the above boundary-value problems, the velocity, free surface elevation and the dynamic pressure can be calculated respectively from

$$\mathbf{v}_j = \nabla\Phi_j, \tag{18}$$

$$\eta_j = \frac{i\omega}{g}\phi_j, \tag{19}$$

$$p_j = -\rho\Phi_{j,t}. \tag{20}$$

Scaled boundary finite-element transformation

In this section, ϕ_1 and ϕ_2^S will both be denoted as ϕ for brevity, and the region Ω_j will be denoted as Ω. If the velocity boundary is defined by Γ_v, we have

$$\phi_{,n} = \bar{v}_n, \quad \text{on} \quad \Gamma_v, \tag{21}$$

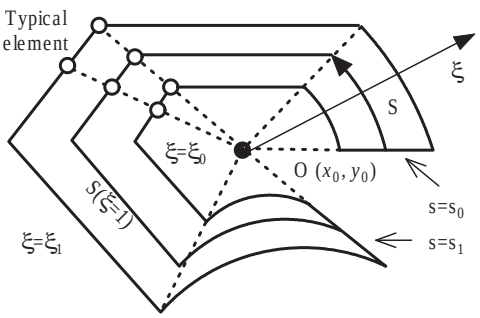

Figure 2: The coordinate definition of SBFEM

where the overbar denotes a prescribed value.

The finite-element method requires the weighted residuals of the governing equation to be zero. Hence Eqs. (11), (14) and (21) are multiplied by a weighting function w and integrated over the flow domain and the boundary. Performing integration by parts, the resulting equation becomes

$$\int_\Omega \nabla^T w\nabla\phi d\Omega - \int_\Omega wk^2\phi d\Omega - \oint_\Gamma w\bar{v}_n d\Gamma = 0. \tag{22}$$

SBFEM defines the domain Ω by scaling a single piecewise-smooth curve S relative to a scaling centre (x_0, y_0), which is chosen at the cylinder centre in this case (see Fig. 2). The circumferential coordinate s is anticlockwise along the curve S and the normalised radial coordinate ξ is a scaling factor, defined as 1 at curve S and 0 at the scaling centre. The whole solution domain Ω is in the range of $\xi_0 \le \xi \le \xi_1$ and $s_0 \le s \le s_1$. The two straight sections $s = s_0$ and $s = s_1$ are called side-faces. They coincide, if the curve S is closed. For bounded domain, $\xi_0 = 0$ and $\xi_1 = 1$; whereas, for unbounded domain, $\xi_0 = 1$ and $\xi_1 = \infty$. Therefore the Cartesian coordinates are transformed to the scaled boundary coordinate ξ and s with the scaling equations

$$x = x_0 + \xi x_s(s), \quad y = y_0 + \xi y_s(s). \tag{23}$$

By employing SBFEM, an approximate solution of ϕ is sought as

$$\phi_A(\xi, s) = \mathbf{N}(s)\mathbf{a}(\xi), \tag{24}$$

where $\mathbf{N}(s)$ is the shape function, the vector $\mathbf{a}(\xi)$ is analogous to the nodal values same as in FEM. The radial function $a_j(\xi)$ represents the variation of the wave potential in the radial axis ξ at each node j, and the shape function $\mathbf{N}(s)$ interpolates between the nodal potential values in the circumferential axis s.

By performing scaled boundary transformation, the operator ∇ can be expressed as [12]:

$$\nabla = \mathbf{b}_1(s)\frac{\partial}{\partial\xi} + \frac{1}{\xi}\mathbf{b}_2(s)\frac{\partial}{\partial s}, \tag{25}$$

where $\mathbf{b}_1(s)$ and $\mathbf{b}_2(s)$ are dependent only on the boundary definition

$$\mathbf{b}_1(s) = \frac{1}{|J|}\begin{Bmatrix} y_s(s)_{,s} \\ -x_s(s)_{,s} \end{Bmatrix}, \qquad \mathbf{b}_2(s) = \frac{1}{|J|}\begin{Bmatrix} -y_s(s) \\ x_s(s) \end{Bmatrix}, \tag{26}$$

and $|J|$ is the Jacobian at the boundary

$$|J| = x_s(s)y_s(s)_{,s} - y_s(s)x_s(s)_{,s}. \tag{27}$$

From Eqs. (18) and (25), the approximate velocity can be expressed as

$$\mathbf{v}_A(\xi,s) = \mathbf{B}_1(s)\mathbf{a}(\xi)_{,\xi} + \frac{1}{\xi}\mathbf{B}_2(s)\mathbf{a}(\xi), \tag{28}$$

where

$$\mathbf{B}_1(s) = \mathbf{b}_1(s)\mathbf{N}(s), \quad \mathbf{B}_2(s) = \mathbf{b}_2(s)\mathbf{N}(s)_{,s}. \tag{29}$$

Applying the Galerkin approach, the weighting function w can be formulated using the same shape function as in Eq. (24)

$$w(\xi,s) = \mathbf{N}(s)\mathbf{w}(\xi) = \mathbf{w}(\xi)^T\mathbf{N}(s)^T. \tag{30}$$

Substituting Eqs. (24), (25), (29) and (30) into Eq. (22) results in

$$\int_\Omega \left[\mathbf{B}_1(s)\mathbf{w}(\xi)_{,\xi} + \frac{1}{\xi}\mathbf{B}_2(s)\mathbf{w}(\xi)\right]^T \left[\mathbf{B}_1(s)\mathbf{a}(\xi)_{,\xi} + \frac{1}{\xi}\mathbf{B}_2(s)\mathbf{a}(\xi)\right] \cdot d\Omega - \int_\Omega k^2\mathbf{w}(\xi)^T\mathbf{N}(s)^T\mathbf{N}(s)\mathbf{a}(\xi)d\Omega - \oint_\Gamma \mathbf{w}(\xi)^T\mathbf{N}(s)^T\bar{v}_n d\Gamma = 0, \tag{31}$$

where the incremental volume [12] is

$$d\Omega = |J|\xi d\xi ds. \tag{32}$$

For convenience, coefficient matrices are introduced here as

$$\mathbf{E}_0 = \int_S \mathbf{B}_1(s)^T\mathbf{B}_1(s)|J|ds, \tag{33}$$

$$\mathbf{E}_1 = \int_S \mathbf{B}_2(s)^T\mathbf{B}_1(s)|J|ds, \tag{34}$$

$$\mathbf{E}_2 = \int_S \mathbf{B}_2(s)^T\mathbf{B}_2(s)|J|ds, \tag{35}$$

$$\mathbf{M}_0 = \int_S \mathbf{N}(s)^T\mathbf{N}(s)|J|ds, \tag{36}$$

$$\mathbf{F}_s(\xi) = \mathbf{N}(s_0)^T(-\bar{v}_n(\xi,s_0))|J(s_0)| + \mathbf{N}(s_1)^T(-\bar{v}_n(\xi,s_1))|J(s_1)|. \tag{37}$$

The above integrals Eqs. (33)-(36) can be computed element by element and assembled together for the entire boundary. Expanding Eq. (31) and integrating the terms containing $\mathbf{w}(\xi)_{,\xi}$ by parts with respect to ξ using Green's theorem leads to

$$\mathbf{w}(\xi_1)^T\left[\mathbf{E}_0\xi_1\mathbf{a}(\xi_1)_{,\xi} + \mathbf{E}_1^T\mathbf{a}(\xi_1) - \int_S \mathbf{N}(s)^T(\bar{v}_n(\xi_1,s))\xi_1 ds\right] - \mathbf{w}(\xi_0)^T\left[\mathbf{E}_0\xi_0\mathbf{a}(\xi_0)_{,\xi} + \mathbf{E}_1^T\mathbf{a}(\xi_0) + \int_S \mathbf{N}(s)^T(\bar{v}_n(\xi_0,s))\xi_0 ds\right] - \int_{\xi_0}^{\xi_1} \mathbf{w}(\xi)^T\Big[\mathbf{E}_0\xi\mathbf{a}(\xi)_{,\xi\xi} + (\mathbf{E}_0 + \mathbf{E}_1^T - \mathbf{E}_1)\mathbf{a}(\xi)_{,\xi} - \mathbf{E}_2\frac{1}{\xi}\mathbf{a}(\xi) + k^2\xi\mathbf{M}_0\mathbf{a}(\xi) - \mathbf{F}_s(\xi)\Big]d\xi = 0. \tag{38}$$

To satisfy all sets of weighting function $\mathbf{w}(\xi)$, the following conditions must be satisfied:

$$\mathbf{E}_0\xi_1\mathbf{a}(\xi_1)_{,\xi} + \mathbf{E}_1^T\mathbf{a}(\xi_1) = \int_S \mathbf{N}(s)^T(\bar{v}_n(\xi_1,s))\xi_1 ds, \tag{39}$$

$$\mathbf{E}_0\xi_0\mathbf{a}(\xi_0)_{,\xi} + \mathbf{E}_1^T\mathbf{a}(\xi_0) = -\int_S \mathbf{N}(s)^T(\bar{v}_n(\xi_0,s))\xi_0 ds, \tag{40}$$

$$\mathbf{E}_0\xi^2\mathbf{a}(\xi)_{,\xi\xi} + (\mathbf{E}_0 + \mathbf{E}_1^T - \mathbf{E}_1)\xi\mathbf{a}(\xi)_{,\xi} - \mathbf{E}_2\mathbf{a}(\xi) + k^2\xi^2\mathbf{M}_0\mathbf{a}(\xi) = \xi\mathbf{F}_s(\xi). \tag{41}$$

Eq. (41) is the so-called scaled boundary finite-element equation. By introducing the shape function, the Helmholtz equation has been weakened in the circumferential direction, so that the governing partial differential equation is transformed to an ordinary matrix differential equation in radial direction. The rank of matrices $\mathbf{E}_0$, $\mathbf{E}_1$, $\mathbf{E}_2$, $\mathbf{M}_0$ and vector $\mathbf{a}(\xi)$ is m (where m is the number of nodes in the curve S). In the present study, the side-faces coincide so that the flow across the side-faces is equal and opposite, leading to vanishing of the term $\mathbf{F}_s(\xi)$. Therefore, the final governing equation, Eq. (41), is a homogeneous second-order ordinary matrix differential equation in terms of matrix of rank m.

Boundary conditions, Eqs. (12) and (13) or Eqs. (15) and (16), are weakened in the form of Eqs. (40) and (39) respectively, indicating the relationship between the integrated nodal flow on the boundary and the velocity potentials of the nodes. For the wave diffraction problem in the unbounded region Ω_2, $\xi_0 = 1$ on the boundary of exterior porous cylinder and $\xi_1 = +\infty$ at infinity. For the boundary-value problem in the bounded annular region Ω_1, $\xi_0 = 0$ and $\xi_1 = 1$.

Solution procedure

For the exterior porous cylinder, we have

$$x_s(s) = b\cos(s/b), \quad y_s(s) = b\sin(s/b). \tag{42}$$

From Eqs. (23), (26), (27), (29) and (33)-(36), $x_s(s)_{,s}$, $y_s(s)_{,s}$, $\mathbf{b}_1(s)$, $\mathbf{b}_2(s)$, $|J|$, $\mathbf{B}_1(s)$, $\mathbf{B}_2(s)$, $\mathbf{E}_0$, $\mathbf{E}_1$, $\mathbf{E}_2$, and $\mathbf{M}_0$ can be calculated accordingly. The following relationships hold:

$$\mathbf{E}_1 = 0\cdot\mathbf{I}, \quad \mathbf{E}_0^{-1}\mathbf{M}_0 = b^2\mathbf{I}, \tag{43}$$

$$\mathbf{E}_0 = \frac{1}{b}\int_S \mathbf{N}(s)^T\mathbf{N}(s)ds, \tag{44}$$

where $\mathbf{I}$ is the identity matrix of rank m.

Using Eq. (43), pre-multiplying both sides of Eq. (41) by $\mathbf{E}_0^{-1}$ and simplifying, we have

$$\zeta^2\mathbf{a}(\zeta)_{,\zeta\zeta} + \zeta\mathbf{a}(\zeta)_{,\zeta} - \mathbf{E}_0^{-1}\mathbf{E}_2\mathbf{a}(\zeta) + \zeta^2\mathbf{a}(\zeta) = 0, \tag{45}$$

where

$$\zeta = kb\xi. \tag{46}$$

Solution for unbounded domain Ω_2

Eq. (45) is the matrix form of Bessel's differential equation. Considering the Sommerfeld radiation condition Eq. (13), it

is logical to select $H_{r_j}(\zeta)\mathbf{T}_j$ as a base solution of Eq. (45) in region Ω_2.

The solution for $\mathbf{a}_2(\zeta)$ is then expressed in the series form:

$$\mathbf{a}_2(\zeta) = \sum_{j=1}^{m} c_j H_{r_j}(\zeta)\mathbf{T}_j = \mathbf{T}\mathbf{H}(\zeta)\mathbf{C}, \tag{47}$$

where $\mathbf{T}_j$ are vectors of rank m, c_j are coefficients, $H_{r_j}(\zeta)$ are the Hankel functions of the first kind, and

$$\mathbf{T} = [\mathbf{T}_1, \mathbf{T}_2, \cdots, \mathbf{T}_m], \tag{48}$$
$$\mathbf{C} = [c_1, c_2, \cdots, c_m]^T, \tag{49}$$
$$\mathbf{H}(\xi) = \mathrm{diag}[H_{r_1}(kb\xi), H_{r_2}(kb\xi), \cdots, H_{r_m}(kb\xi)], \tag{50}$$

where "diag" denotes a diagonal matrix with the elements in the square brackets on the main diagonal.

Substituting Eq. (47) into Eq. (45), and using the following properties of Hankel function

$$\zeta^2 H''_{r_j}(\zeta) = -\zeta^2 H_{r_j}(\zeta) + \zeta H_{r_j+1}(\zeta) - r_j H_{r_j}(\zeta) + r_j^2 H_{r_j}(\zeta), \tag{51}$$
$$\zeta H'_{r_j}(\zeta) = -\zeta H_{r_j+1}(\zeta) + r_j H_{r_j}(\zeta), \tag{52}$$

where the prime and the double prime denote the first and second derivatives with respect to the argument ζ respectively, we have

$$\sum_{j=1}^{m} (\mathbf{E}_0^{-1}\mathbf{E}_2 - r_j^2\mathbf{I})\mathbf{T}_j \cdot c_j H_{r_j}(\zeta) = 0. \tag{53}$$

For any $c_j H_{r_j}(\zeta)$, Eq. (53) yields

$$(\mathbf{E}_0^{-1}\mathbf{E}_2 - r_j^2\mathbf{I})\mathbf{T}_j = 0. \tag{54}$$

Let λ_j be the eigenvalues of $\mathbf{E}_0^{-1}\mathbf{E}_2$, then $r_j = \sqrt{\lambda_j}$, and $\mathbf{T}_j$ are the eigenvectors of $\mathbf{E}_0^{-1}\mathbf{E}_2$.

Since the Sommerfeld radiation condition (13) or (39) has been satisfied by the Hankel functions, we now only consider the body boundary condition (40) of the circular cylinder

$$\mathbf{E}_0 kb \sum_{j=1}^{m} c_j H'_{r_j}(kb)\mathbf{T}_j = -\left[\int_S \mathbf{N}(s)^T \mathbf{N}(s) ds\right] \bar{\mathbf{v}}_{2n}^S, \tag{55}$$

where $\bar{\mathbf{v}}_{2n}^S$ is the vector of nodal normal velocity of scattered wave in region Ω_2 on the body boundary.

Solution for bounded domain Ω_1

Similar approach is applied to the region Ω_1. Assume

$$\mathbf{a}_1(\zeta) = \sum_{j=1}^{m} [c_j^1 J_{r_j}(\zeta) + c_j^2 Y_{r_j}(\zeta)]\mathbf{T}_j = \mathbf{T}[\mathbf{J}(\zeta)\mathbf{C}^1 + \mathbf{Y}(\zeta)\mathbf{C}^2], \tag{56}$$

where c_j^1 and c_j^2 are coefficients, $J_{r_j}(\zeta)$ are the Bessel functions of the first kind, $Y_{r_j}(\zeta)$ are the Bessel functions of the second kind, and

$$\mathbf{C}^1 = [c_1^1, c_2^1, \cdots, c_m^1]^T, \tag{57}$$
$$\mathbf{C}^2 = [c_1^2, c_2^2, \cdots, c_m^2]^T, \tag{58}$$
$$\mathbf{J}(\xi) = \mathrm{diag}[J_{r_1}(kb\xi), J_{r_2}(kb\xi), \cdots, J_{r_m}(kb\xi)], \tag{59}$$
$$\mathbf{Y}(\xi) = \mathrm{diag}[Y_{r_1}(kb\xi), Y_{r_2}(kb\xi), \cdots, Y_{r_m}(kb\xi)]. \tag{60}$$

Again if λ_j are the eigenvalues of $\mathbf{E}_0^{-1}\mathbf{E}_2$, then $r_j = \sqrt{\lambda_j}$, and $\mathbf{T}$ is the eigenvector of $\mathbf{E}_0^{-1}\mathbf{E}_2$.

Applying boundary conditions on the interior cylinder Eq. (40) and the exterior porous cylinder Eq. (39), respectively, we have

$$\mathbf{C}^2 = -\mathbf{Y}_a'^{-1}\mathbf{J}_a'\mathbf{C}^1, \tag{61}$$

$$\mathbf{E}_0 kb\mathbf{T}(\mathbf{J}_b'\mathbf{C}^1 + \mathbf{Y}_b'\mathbf{C}^2) = \left[\int_S \mathbf{N}(s)^T \mathbf{N}(s) ds\right] \bar{\mathbf{v}}_{1n}, \tag{62}$$

where $\bar{\mathbf{v}}_{1n}$ is the vector of nodal total normal velocity in region Ω_1 on the body boundary of exterior cylinder.

Combining Eqs. (10), (21), (24), (44), (47), (55), (56) and (62), and noting

$$\bar{\mathbf{v}}_{2n}^I + \bar{\mathbf{v}}_{2n}^S = \bar{\mathbf{v}}_{2n} = -\bar{\mathbf{v}}_{1n}, \tag{63}$$

where $\bar{\mathbf{v}}_{2n}^I$ is the vector of nodal normal velocity of incident wave in the region Ω_2 on the body boundary of the exterior cylinder, $\mathbf{a}_1(\xi)$ and $\mathbf{a}_2(\xi)$ are solved as

$$\mathbf{a}_1(\xi) = \mathbf{T}[\mathbf{J}(\xi)\mathbf{Y}_a' - \mathbf{Y}(\xi)\mathbf{J}_a']\mathbf{W}^{-1}(\mathbf{T}^{-1}\bar{\mathbf{a}}_2^I + \mathbf{H}_{bh}\mathbf{T}^{-1}\bar{\mathbf{v}}_{2n}^I/k), \tag{64}$$

$$\mathbf{a}_2(\xi) = \mathbf{T}\mathbf{H}_h(\xi)\mathbf{W}^{-1}[(\mathbf{J}_b'\mathbf{Y}_a' - \mathbf{Y}_b'\mathbf{J}_a')\mathbf{T}^{-1}\bar{\mathbf{a}}_2^I + \mathbf{V}\mathbf{T}^{-1}\bar{\mathbf{v}}_{2n}^I/k], \tag{65}$$

where

$$\mathbf{V} = -\frac{1}{iG}(\mathbf{J}_b'\mathbf{Y}_a' - \mathbf{Y}_b'\mathbf{J}_a') + (\mathbf{J}_b\mathbf{Y}_a' - \mathbf{Y}_b\mathbf{J}_a'), \tag{66}$$
$$\mathbf{W} = \mathbf{V} - \mathbf{H}_{bh}(\mathbf{J}_b'\mathbf{Y}_a' - \mathbf{Y}_b'\mathbf{J}_a'), \tag{67}$$

and

$$\mathbf{J}_a' = \mathrm{diag}[J'_{r_1}(ka), J'_{r_2}(ka), \cdots, J'_{r_m}(ka)], \tag{68}$$
$$\mathbf{Y}_a' = \mathrm{diag}[Y'_{r_1}(ka), Y'_{r_2}(ka), \cdots, Y'_{r_m}(ka)], \tag{69}$$
$$\mathbf{J}_b = \mathrm{diag}[J_{r_1}(kb), J_{r_2}(kb), \cdots, J_{r_m}(kb)], \tag{70}$$
$$\mathbf{Y}_b = \mathrm{diag}[Y_{r_1}(kb), Y_{r_2}(kb), \cdots, Y_{r_m}(kb)], \tag{71}$$
$$\mathbf{J}_b' = \mathrm{diag}[J'_{r_1}(kb), J'_{r_2}(kb), \cdots, J'_{r_m}(kb)], \tag{72}$$
$$\mathbf{Y}_b' = \mathrm{diag}[Y'_{r_1}(kb), Y'_{r_2}(kb), \cdots, Y'_{r_m}(kb)], \tag{73}$$

$$\mathbf{H}_h(\xi) = \mathrm{diag}[H_{r_1}(kb\xi)/H'_{r_1}(kb), \cdots, H_{r_m}(kb\xi)/H'_{r_m}(kb)], \tag{74}$$

$$\mathbf{H}_{bh} = \mathrm{diag}[H_{r_1}(kb)/H'_{r_1}(kb), \cdots, H_{r_m}(kb)/H'_{r_m}(kb)]. \tag{75}$$

For the limiting case of short-crested wave interacting with a hollow porous cylinder, i.e. $a = 0$, $\mathbf{a}_1(\xi)$ and $\mathbf{a}_2(\xi)$ are

$$\mathbf{a}_1(\xi) = \mathbf{T}\mathbf{J}(\xi)\mathbf{W}^{-1}(\mathbf{T}^{-1}\bar{\mathbf{a}}_2^I + \mathbf{H}_{bh}\mathbf{T}^{-1}\bar{\mathbf{v}}_{2n}^I/k), \tag{76}$$

$$\mathbf{a}_2(\xi) = \mathbf{T}\mathbf{H}_h(\xi)\mathbf{W}^{-1}(\mathbf{J}'_b\mathbf{T}^{-1}\bar{\mathbf{a}}_2^I + \mathbf{V}\mathbf{T}^{-1}\bar{\mathbf{v}}_{2n}^I/k), \tag{77}$$

where

$$\mathbf{V} = -\frac{1}{iG}\mathbf{J}'_b + \mathbf{J}_b, \tag{78}$$

$$\mathbf{W} = \mathbf{V} - \mathbf{H}_{bh}\mathbf{J}'_b. \tag{79}$$

Using Eqs. (4), (5), (17), (21) and (24), $\bar{\mathbf{v}}_{2n}^I$ and $\bar{\mathbf{a}}_2^I$ can be easily determined on the exterior cylinder boundary. From Eqs. (6), (9), (24), (64) and (65), the approximation of velocity potential in both region Ω_1 and region Ω_2 can be obtained.

All the other physical properties of engineering interest including velocity, surface elevation, and pressure can now be determined based on the velocity potentials by Eqs. (18)-(20). The total force per unit length on the cylinder in the principal direction of wave propagation is then calculated as:

$$\frac{dF_x}{dz} = -R\int_0^{2\pi} p\cdot\cos(\alpha)d\alpha = 2\pi R P_x(k_x,k_y,k,R)\cdot\rho g A\cdot Z(z)e^{-i\omega t}, \tag{80}$$

$$\frac{dF_y}{dz} = -R\int_0^{2\pi} p\cdot\sin(\alpha)d\alpha = 2\pi R P_y(k_x,k_y,k,R)\cdot\rho g A\cdot Z(z)e^{-i\omega t}, \tag{81}$$

where the function $P_u(k_x,k_y,k,R)$ $(u = x,y)$ is the dimensionless parameter of dF_u/dz without the term $\rho g A\cdot Z(z)e^{-i\omega t}$ and R is the radius of the cylinder (a or b).

The function $P_u(k_x,k_y,k,R)$ determines the first-order total horizontal force in u direction on the cylinder, F_u, which can be obtained by integrating Eqs. (80) and (81) with respect to z,

$$F_u = \int_{-h}^{0}\frac{dF_u}{dz}dz = 2\pi R P_u(k_x,k_y,k,R)\cdot\rho g A e^{-i\omega t}\cdot\tanh(kh)/k. \tag{82}$$

It can be concluded from Eq. (82) that only the function $P_u(k_x,k_y,k,R)$ needs to be discussed.

Results and Discussion

The effects of the short-crested phase θ on total horizontal forces, horizontal wave force components in x and y directions and wave runups around the cylinders are calculated and the results are plotted in Figures 3, 4, and 5 respectively. The parameters are $G_0 = 1$, $a = 1$ m, $b = 2$ m, $k = 1$ m^{-1}. Five cases with the same total wave number k are presented in Figure 3, i.e., (1) $k_x = 1$ m^{-1}, $k_y = 0$ m^{-1}; (2) $k_x = 0.8$ m^{-1}, $k_y = 0.6$ m^{-1}; (3) $k_x = \sqrt{2}/2$ m^{-1}, $k_y = \sqrt{2}/2$ m^{-1}; (4) $k_x = 0.6$ m^{-1}, $k_y = 0.8$ m^{-1}; (5) $k_x = 0$ m^{-1}, $k_y = 1$ m^{-1}. Four typical cases (1), (2), (3) and (5) shown in Figure 4 represent the wave force components in x and y directions. In Figure 5, wave numbers are fixed as $k_x = \sqrt{2}/2$ m^{-1}, $k_y = \sqrt{2}/2$ m^{-1}. Runups are calculated on 12 points (polar angle $\alpha = 0, \pi/2, \pi, 3\pi/2$) around inner and outer cylinders, where the outer cylinder has runups in two sides (in Ω_1 and Ω_2). 16 and 32 three-noded quadratic elements are used in circumference of the outer cylinder to calculate the wave forces and runups respectively.

It can be seen from Figures 3, 4 and 5 that the wave forces and runups fluctuate at a period π as the short-crested phase varies. The maximum wave forces occur when the incident wave is a plane or standing wave. The wave forces in u $(u = x,y)$ direction are proportional to the wave numbers in u direction if ka and kb are fixed. The total horizontal forces, however, are dependent on both k_x and k_y. For a plane and standing incident wave, the total horizontal forces vanish at $\theta = \pi/2, 3\pi/2$ and $\theta = 0, \pi$ respectively. However, for short-crested incident waves ($k_x, k_y \neq 0$), the zero total horizontal force will never occur. For the incident wave with the wave number $k_x < k_y$, the highest wave forces occur for the incident waves at $\theta = \pi/2, 3\pi/2$, where the wave forces induced by plane waves vanish.

As for the runups, it can be seen in Figures 5, the incident waves with the equal wave numbers in both x and y directions tends to result the largest elevation in the weather side and the smallest elevation in the lee side. The runups in the outer region Ω_2 are usually larger than their counterparts in annular region Ω_1 except the runups in the lee side. It can be concluded that the porous structure can effectively reduce the wave impacts on the coastal and offshore structures in terms of reducing wave forces and wave runups on the structure.

Conclusions

The semi-analytical scaled boundary finite-element method has been successfully applied to solve the diffraction of short-crested waves by a concentric porous cylinder system. The effect of the short-crested phase θ on wave forces and runups are discussed. It is found that the wave forces and runups fluctuate periodically as the short-crested phase varies. The maximum wave forces occur at an incident plane or standing wave. Maximum wave forces may arise other than short-crested phase $\theta = 0$, thus the effect of short-crested phase must be considered. The runups in the outer region are usually larger than their counterparts in annular region except in the lee side. It is demonstrated that the porous structure can effectively reduce the wave impacts on the coastal and offshore structures. The SBFEM method holds promise in solving more practical coastal and ocean engineering problems.

Acknowledgements

This paper is based on the project funded by Australian Research Council (ARC) under Discovery Project Grant No. DP0450906. Authors would like to thank the financial support from ARC.

References

[1] Chwang, A.T., A Porous Wavemaker Theory, *J. Fluid Mech.*, **132**, 1983, 395–406.

[2] Chwang, A.T. and Chan, A.T., Interaction between Porous Media and Wave Motion, *Annu. Rev. Fluid Mech.*, **30**, 1998,

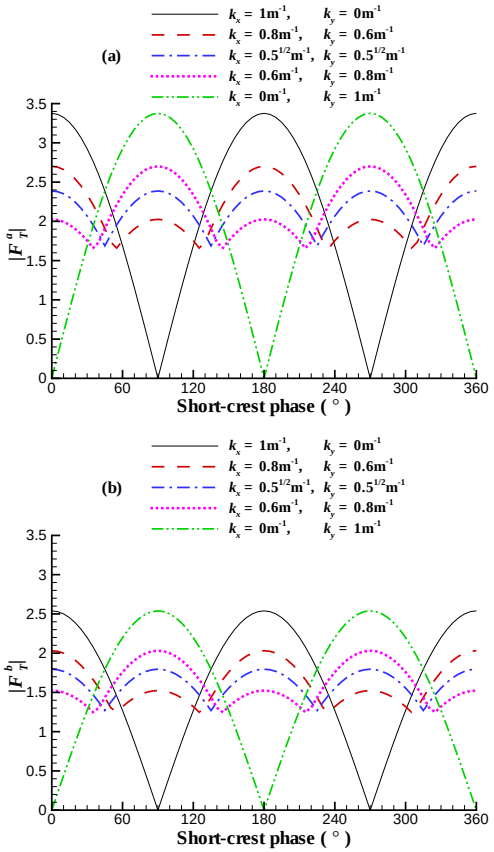

Figure 3: Variations of the total horizontal forces of interior and exterior cylinders *vs* the short-crested phase θ.

53–84.

[3] Darwiche, M.K.M., Williams, A.N. and Wang, K.H., Wave Interaction with Semiporous Cylindrical Breakwater, *J. Waterway, Port, Coastal, Ocean Eng.*, **120**, 1994, 382–403.

[4] Li, B., Cheng, L., Deeks, A.J. and Zhao, M., A Semi-analytical Solution Method for Two-Dimensional Helmholtz Equation, *Appl. Ocean Res.*, **28**, 2006, 193–207.

[5] Song, Ch. and Wolf, J.P., The Scaled Boundary Finite-Element Method - Alias Consistent Infinitesimal Finite-Element Cell Method - for Elastodynamics, *Comput. Method Appl. M.*, **147**, 1997, 329–355.

[6] Tao, L., Song, H. and Chakrabarti, S., Scaled Boundary FEM Solution of Short-Crested Wave Diffraction by a Vertical Cylinder, *Comput. Method Appl. M.*, 2007, doi:10.1016/j.cma.2007.07.025.

[7] Taylor, G., Fluid Flow in Regions Bounded by Porous Surfaces, *P. Roy. Soc. Lond. A Mat.*, **234**, 1956, 456–475.

[8] Tsai, C.P., Jeng, D.S. and Hsu, J.R.C., Computations of the Almost Highest Short-crested Waves in Deep Water, *Appl. Ocean Res.*, **16**, 1994, 317–326.

[9] Wang, K.H. and Ren, X., Water Waves on Flexible and Porous Breakwater, *J. Eng. Mech.*, **119**, 1993, 1025–1047.

[10] Wang, K.H. and Ren, X., Wave Interaction with a Concentric Porous Cylinder System, *Ocean Eng.*, **21**, 1994, 343–360.

[11] Williams, A.N. and Li, W., Wave Interaction with a Semi-Porous Cylindrical Breakwater Mounted on a Storage Tank, *Ocean Eng.*, **25**, 1998, 195–219.

[12] Wolf, J.P., *The Scaled Boundary Finite Element Method*, John Wiley & Sons Ltd, 2003.

[13] Yu, X. and Chwang, A.T., Wave-Induced Oscillation in Harbor with Porous Breakwaters, *J. Waterway, Port, Coastal, Ocean Eng.*, **120**, 1994, 125–144.

[14] Yu, X. and Chwang, A.T., Wave Motion through Porous Structures, *J. Eng. Mech.*, **120**, 1994, 989–1008.

[15] Zhu, S., Diffraction of Short-crested Waves around a Circular Cylinder, *Ocean Eng.*, **20**, 1993, 389–407.

[16] Zhu, S. and Moule, G., Numerical Calculation of Forces Induced by Short-Crested Waves on a Vertical Cylinder of Arbitrary Cross-Section, *Ocean Eng.*, **21**, 1994, 645–662.

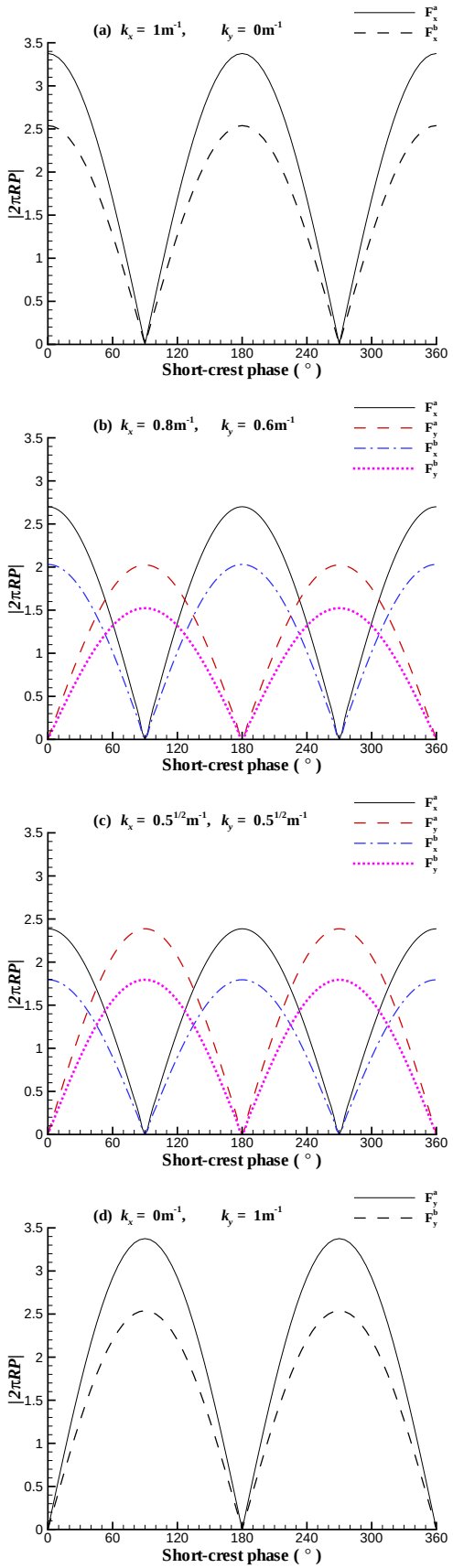

Figure 4: Variations of the horizontal forces *vs* the short-crested phase θ.

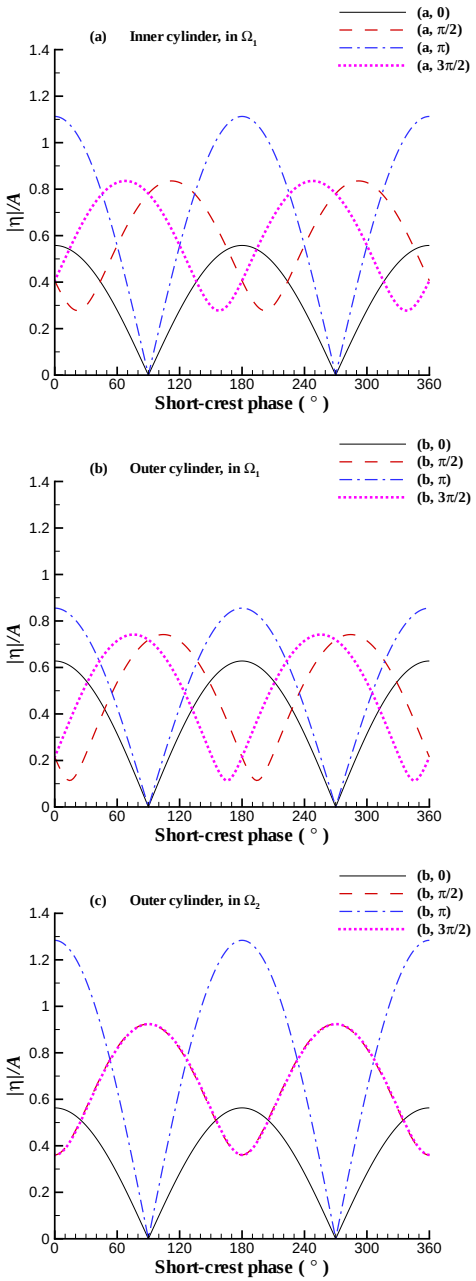

Figure 5: Variations of the wave runups *vs* the short-crested phase θ.